Heliyon 7 (2021) e07537

Contents lists available at ScienceDirect

Heliyon

journal homepage: www.cell.com/heliyon

Research article

Nanoencapsulation of basil essential oil alleviates the oxidative stress, genotoxicity and DNA damage in rats exposed to biosynthesized iron nanoparticles

Aziza A. El-Nekeety [a], Marwa E. Hassan [b], Rasha R. Hassan [c], Ola I. Elshafey [d], Zeinab K. Hamza [a], Sekena H. Abdel-Aziem [e], Nabila S. Hassan [f], Mosaad A. Abdel-Wahhab [a,*]

[a] Food Toxicology & Contaminants Dept., National Research Centre, Dokki, Cairo, Egypt
[b] Toxicology Dept., Research Institute of Medical Entomology, Giza, Egypt
[c] Immunology Dept., Research Institute of Medical Entomology, Giza, Egypt
[d] Physical Chemistry Dept., National Research Centre, Dokki, Cairo, Egypt
[e] Cell Biology Dept., National Research Centre, Dokki, Cairo, Egypt
[f] Pathology Dept. National Research Centre, Dokki, Cairo, Egypt

ARTICLE INFO

Keywords:
Nanotechnology
Iron nanoparticles
Encapsulated basil oil
DNA fragmentation
Oxidative stress
Genotoxicity

ABSTRACT

The application of essential oils in food and pharmaceutical sectors face several challenges due to their sensitivity to oxidation process. Additionally, the biosynthesis of nanometals is growing rapidly; however, the toxicity of these particles against living organisms did not well explore yet. This study aimed to determine the bioactive compounds in basil essential oil (BEO) using GC-MS, to encapsulate and characterize BEO and to evaluate its protective role against the oxidative stress and genotoxicity of biosynthesized iron nanoparticles (Fe-NPs) in rats. Six groups of male Sprague-Dawley rats were treated orally for 4 weeks included the control group, Fe-NPs-treated group (100 mg/kg b.w.); EBEO-treated groups at low (100 mg/kg b.w.) or high (200 mg/kg b.w.) dose and the groups treated with Fe-NPs plus the low or the high dose of EBEO. The GC-MS analysis revealed the identification of 48 compounds and linalool was the major compound. The average sizes and zeta potential of the synthesized Fe-NPs and EBEO were 60 ± 4.76 and 120 ± 3.2 nm and 42.42 mV and -6.4 mV, respectively. Animals treated with Fe-NPs showed significant increase in serum biochemical analysis, oxidative stress markers, cytokines, lipid profile, DNA fragmentation and antioxidant enzymes and their gene expression and severe changes in the histology of liver and kidney tissues. Administration of Fe-NPs plus EBEO alleviated these disturbances and the high dose could normalize most of the tested parameters and improved the histology of liver and kidney. It could be concluded that caution should be taken in using the biosynthesized metal nanoparticles in different application. EBEO is a potent candidate to protect against the hazards of metal nanoparticles and can be applied in food and medical applications.

1. Introduction

Nowadays, nanotechnology seems a promising revolution in the construction and characterization of the functional properties of the nanoparticles to incur into different branches of sciences (Jothirethinam et al., 2015). Basil *(Ocimum basilicum L)* is an herb widely used in folk medicine, food flavoring. The essential oil of basil is rich in terpenoid and phenolic components (Chitprasert and Sutaphanit, 2014). This oil has several health benefits such as enhance digestion and inhibit cholesterol synthesis (Majdi et al., 2020), antioxidant (Rezzoug et al., 2019), anti-inflammatory (Eftekhar et al., 2019), antimicrobial (Ebani et al., 2018), anthelmintic (Dawood et al., 2021), and chemopreventive agents (Fitsiou and Pappa, 2019). However, the challenge of using essential oil for any application is to maintain its chemical stability. These essential oils are unstable to oxygen, temperature, light, water content and pH (Aguilar-Veloz et al., 2020; Sandra et al., 2019; Fitsiou and Pappa, 2019). Therefore, a system offering essential oil protection against these deterioration factors is required. Encapsulation technique is an attractive method for the protection of the active components in these essential oils and also to improve their delivery and controlled release in the core of

* Corresponding author.
E-mail addresses: mosaad_abdelwahhab@yahoo.com, ma.abdelwahab@nrc.Sc.eg (M.A. Abdel-Wahhab).

https://doi.org/10.1016/j.heliyon.2021.e07537
Received 15 May 2021; Received in revised form 27 June 2021; Accepted 7 July 2021

the nano-capsule structure of membrane wall (Abdel-Wahhab et al., 2018; Lammari et al., 2020).

Nanometals (NMs) have specific potentials based on their bioavailability, enhanced absorption, and the ability to cross biological barriers (Wang et al., 2010). The toxicity of NMs is extensively reported *in vitro* models (Dönmez Güngüneş et al., 2017) such as delayed the development and maturation in rabbits and mice (Noori et al., 2011), embryonic malformations, and mortality in the embryos of zebrafish (Zhu et al., 2012). Iron oxide nanoparticles (Fe-NPs) are widely used for different biomedical and bioengineering applications including cell labeling and cancer therapy (Zhu et al., 2017), drug delivery and magnetic resonance imaging (Dadfar et al., 2019; Mohammed et al., 2017). Moreover, iron works as a double-edged sword where it is used as a food supplement at fairly low levels but if its level exceeds the range of human tolerance, toxic effects such as nausea, celialgia, and even death occurred (Ajinkya et al., 2020).

Despite these beneficial effects of Fe-NPs, several studies reported that Fe-NPs generate reactive oxygen species (ROS)-mediated toxicity and peroxidation of lipid membrane (Fernández-Bertólez et al., 2019; Malhotra et al., 2020). Contradicting research reports on the toxicity of Fe-NPs include low-grade toxicity with intracellular ROS generation (Yarjanli et al., 2017) or absence of any form of toxicity at lower doses (Malhotra et al., 2020). However, higher doses of Fe-NPs cause a decline in cellular physiological functions primarily due to oxidative damage of DNA (Florencia et al., 2016), gene transcription modulation, mitochondrial damage, and altered calcium-dependent signaling cascade (Krzywoszyńska et al., 2020). There is public concern regarding the toxicity and adverse effect of NMs on human health and the environment. However, the reports on their toxicological effects on the environment and humans are scarce; thus, the need for a proper solution for NMs toxicity is an urgent demand. The current study aimed to determine the bioactive compounds in basil essential oil using GC-MS, preparation and characterization of encapsulated basil essential oil (EBEO) and determination of the potential protective role of EBEO against the oxidative stress and genotoxicity of biosynthesized Fe-NPs in rats.

2. Materials and methods

2.1. Chemicals and kits

Ferrous sulfate heptahydrate ($FeSO_4.7H_2O$) was purchased from Sigma Chemical Co. (St Louis, MO, USA). Kits for triglycerides (TG), cholesterol (Cho), high-density lipoprotein (HDL), low-density lipoprotein (LDL), total protein (TP), creatinine, urea alanine aminotransferase (ALT) and aspartate aminotransferase (AST) were supplied by FAR Diagnostics Company (Via Fermi, Italy). Kits for nitric oxide (NO), Catalase (CAT), glutathione peroxidase (GPx) and superoxide dismutase (SOD) were supplied by Eagle diagnostics (Dallas, TX, USA). However, malondialdehyde (MDA) kits were supplied by OxisResearch™ Co. (USA). Tumor necrosis factor-alpha (TNF-α) ELISA kit was supplied by Orgenium Laboratories (Helsinki, Finland). Alpha-fetoprotein (AFP) ELISA kit was supplied by BioChem ImmunoSystems Canada Inc. (Montreal, Canada). Carcinoembryonic antigen (CEA) ELISA kit was supplied by Bio diagnostic (Giza, Egypt). TRIZOL was supplied by Invitrogen™ (CA, USA). All other chemicals used were of the highest analytical grade available.

2.2. Basil essential oil (BEO) extraction

The essential oil of basil was extracted using Clevenger-type apparatus as described by Alsaraf et al. (2020) and was dried over anhydrous sodium sulfate then stored at 4 °C until used.

2.3. GC-MS analysis of BEO

The analysis of BEO was carried out by Hewlett-Packard GC-MS model 5890 with a flame ionization detector (FID) and DB-5 fused silica capillary column (60 m × 0.32 mm) using the conditions described in details in our previous work (Hassan et al., 2021). Kovats index of the volatile components were calculated according to Adams (2007) using hydrocarbons as references (C7–C20, Aldrich Co).

2.4. Preparation of encapsulated basil essential oil (EBEO)

The encapsulation of BEO was carried out using whey protein isolate (WPI) and tween 80 (80 mg) as an emulsifier according to Jinapong et al. (2008). The emulsion solution was encapsulated by spray drying.

2.5. Synthesis of iron nanoparticles (Fe-NPs)

Fresh leaves of holy basil were collected from the agriculture area in Dakahlia governorate, Egypt and were washed thoroughly with deionized water then dried at room temperature. The aqueous extract of the leaves was prepared using 12 mg of the dried leaves in 50 ml deionized water in a temperature-controlled water bath at 80 °C. After 1 h, the mixture was filtered and used for the synthesis of Fe-NPs as described by Wonsawat and Panprom (2016). $FeSO_4$ (0.1 mol/L) was mixed with the extract with a volume ratio 5:1 and stirred until the color of the solution turned to dark brown indicating the reduction of Fe^{2+}. The Fe-NPs were collected by centrifugation at 10000 rpm (10 min), washed with distilled water and sonicated several times before subjected to centrifugation again. The collected Fe-NPs were then dried at 90 °C and the powder was used for further experiments.

2.6. Characterization of Fe-NPs and EBEO

Scanning electron micrographs (SEM) were recorded on JEOL JAX-840A and JEOL JEM- 1230 electron micro-analyzers, respectively. The Fe-NPs samples were scattered in ethanol and then treated ultrasonically to disperse the individual particle over the gold grids. However, the SEM analysis of EBEO was carried out as described in details in our previous work (Hassan et al., 2021) and an Orius 1000 CCD camera (GATAN, Warrendale, PA, USA) was used for image acquisition. Zeta potential was determined for Fe-NPs or EBEO immediately after being sonicated for 30–60 min. The size distribution, average diameter, and zeta potential of Fe-NPs and EBEO were determined by a particle size analyzer (Nano-ZS, Malvern Instruments Ltd., UK).

2.7. Experimental animals

Three-month-old sexually mature female Sprague-Dawley rats (150–160 g) were obtained from the Animal House Lab, National Research Center (NRC), Dokki, Cairo, Egypt. The animals were fed on a standard pellet diet and kept under suitable conditions for one week for adaptation. The animals were maintained in filter top polycarbonate cages in a good validation room free from any source of chemical contamination, under normal temperature (25 ± 1 °C) and 12:12-h dark-light cycle at the Animal House Lab, NRC. The protocol of the study was approved by the Committee of Scientific Ethics ate NRC, Dokki, Cairo, Egypt and was carried out following the guidelines of National Institute of Health (NIH publication 86-23 revised 1985).

2.8. Experimental design

Six groups of animals (10 rats/group) were treated orally for 28 days using a stomach tube as follows: group 1; normal control animals which received saline, group 2; rats treated with an aqueous solution of Fe-NPs (100 mg/kg b.w), groups 3 and 4, rats treated with low dose (LD) or high dose (HD) of an aqueous solution of EBEO (100 and 200 mg/kg b.w, respectively), groups 5 and 6; rats treated with Fe-NPs plus EBEO (LD) or EBEO (HD). At the end of the treatment period, all animals have fasted for 12 h, then blood samples were collected via the retro-orbital venous plexus under isoflurane anesthesia. Sera were separated using cooling

centrifugation and stored at -20 °C until analysis of ALT, AST, TP, creatinine, urea, lipid profile, AFP, TNF-α and CEA according to the kit's instructions. After the collection of blood samples, animals were euthanized and samples of the liver and kidney of each animal were dissected, weighed and homogenized in phosphate buffer (pH 7.4) and the supernatant was used for the determination of MDA, and NO, GPx, CAT and SOD according to Lin et al. (1998). Another sample of each organ from each animal was fixed in 10% neutral formalin and paraffin-embedded. Sections (5 μm thickness) were stained with hematoxylin and eosin (H & E) for the histological examination (Bancroft et al., 1996). A sample of the liver from each animal was kept at -80 °C for gene expression analysis.

2.9. Cytogenetic analyses

2.9.1. RNA isolation and RT-PCR analysis

Total RNA was isolated from liver specimens using TRIZOL reagent according to the instructions of the manufacturer. The extracted RNA was dissolved in 30 μL nuclease-free distilled water and stored at -80 °C until used. The purity and concentration of RNA were determined by NanoDrop™ 1000 Spectrophotometer (Thermo Fisher Scientific, USA). The integrity of the RNA was confirmed with agarose gel electrophoresis. RNase-free DNase kit (Promega) was used to remove any DNA contamination. Total RNA (1μg) was converted to cDNA using a PreMix cDNA Kit (iNtRON Biotechnology, Korea). The resulting cDNA was stored at 20°C for later use or directly used as a semi-quantitative PCR template. The expression of the selected genes was quantified using quantitative real-time PCR performed in a One-Step SYBR Select Master Mix Kit as previously described (Kim et al., 2009). The gene-specific primer sequences for GAPDH, GPx, SOD and CAT are shown in Table 1. Real-time quantitative PCR (RT-qPCR) was carried out on Stratagene Mx3005P Real-Time PCR System (Agilent Technologies) in a 20-μL reaction volume using, 1 μL cDNA, 10 μM of forward and reverse primers, 10 μL TOP real™ qPCR 2× Pre MIX (SYBR Green with low ROX) (Enzynomics) and DNAse-free water. All samples were amplified in a minimum of triplicates. Amplification was performed with a 15-min denaturation at 95 °C, then 40 cycles of 95 °C for 12 s, 58–63 °C for 15 s, and 72 °C for 30 s. To assess amplification specificity, melting curve analysis was performed. Relative gene expression levels normalized to GAPDH were calculated using the $2-\Delta\Delta Ct$ method according to Livak and Schmittgen (2001) and El-makawy et al. (2020).

2.9.2. DNA fragmentation assays for apoptosis

The changes in apoptotic of the liver tissue were assayed colorimetrically by the DNA fragmentation and by the agarose gel electrophoresis following the method of Lu et al. (2002).

2.9.3. DNA gel electrophoresis laddering assay

DNA was electrophoresed using agarose gels (1%) containing ethidium bromide (0.71 g/ml) and the gels were then examined by UV transillumination. The reaction of diphenyl amine (DPA) assay was applied for the detection of fragmented and intact DNA as suggested by Gibb et al. (1997) and modified by Abdel-Wahhab et al. (2017).

2.10. Statistical analysis

Statistical analyses were carried using SPSS 16. Data were expressed as mean ± SE. Variables were compared using one-way ANOVA; post hoc Duncan's test and the significance of differences among means were determined at $p \leq 0.05$.

3. Results

The GC-MS results of BEEO (Table 2) revealed the isolation of 48 compounds representing 98.8 % of the oil. The eight major compounds represented 74.4% of the oil were linalool (42.1%), 1,8-Cineole (7.8%), (z)-isoeugeno (6.3%), α-trans-bergamotene (4.9%), 1-epi-cubenol (4.6%), (Z)-Anethole (3.8%), trans-muurola-4-(14),5-diene (2.6%) and ϵ-Caryophyllene (2.3%); however, the other compounds were found in a concentration less than 2% (Table 2).

The characterizations of Fe-NPs and EBEO are detailed in Figure 1. The synthesized Fe-NPs showed a spherical shape (Figure 1A) with an average particle size 60 ± 4.76 nm (Figure 1B) and a zeta potential of 42.42 mV (Figure 1C). However, the synthesized EBEO showed a smooth rounded shape (Figure 1D) with an average size of 120 ± 3.2 nm (Figure 1E) and a zeta potential of -6.4 mV (Figure 1F).

The effect of EBEO on the body weight of animals exposed to Fe-NPs and/or EBEO is presented in Figure 2. Animals treated with Fe-NPs lost weight; however, no significant change in body weight was noticed in the groups administrated EBEO (LD) or EBEO (HD) compared with the control animals. Animals administrated Fe-NPs plus EBEO gained weight and the final body weight was higher than the control but no difference was noticed between those received the low or high dose.

The results of liver and kidney function (Table 3) showed that administration of Fe-NPs induced a significant increase in AST, ALT, creatinine and urea; however; TP was significantly decreased. EBEO at the two doses did induce significant effects of these parameters. The combined administration with Fe-NPs plus EBEO improved the biochemical parameters and EBEO (HD) could normalize them. Additionally, the data given in Table 4 showed that Fe-NPs administration increased ($p < 0.05$) cholesterol, TG and LDL and decreased ($p < 0.05$) HDL. Treatment with EBEO at both dose levels did not affect lipid profile parameters except HDL which was increased significantly in a dose-dependent. Co-administration of Fe-NPs plus EBEO could normalize all lipid parameters except TG level in rats treated with Fe-NPs plus EBEO (LD) which was significantly decreased compare to the control group.

The current results also revealed that AFP, TNF-α and CEA were increased ($p < 0.05$) in rats that administrated Fe-NPs (Table 5). EBEO did not affect these cytokines at the low or the high dose; however, co-administration of EBEO and Fe-NPs significantly improved these cytokines and could normalize TNF-α, and CEA at the high dose. Additionally, administration of Fe-NPs induced oxidative damage in the renal and hepatic tissue as manifested by the significant increase of hepatic MDA and NO (Table 6). Treatment with EBEO (LD) or EBEO (HD) did not affect NO or MDA in both organs except NO in the kidney which was higher than the control level. The combined treatment restored this elevation of MDA and NO and EBEO (LD) could normalize renal NO and hepatic MDA; however, EBEO (HD) could normalize hepatic and renal NO, hepatic MDA and decreased renal MDA than the untreated control group. The results of hepatic and renal antioxidant enzyme activity (Table 7) indicated that Fe-NPs decreased ($p < 0.05$) hepatic and renal GPx, CAT, and SOD. Treatment with EBEO (LD) did not induce a significant effect on these enzymes; however, EBEO (HD) increased hepatic GPx, CAT and SOD and only SOD in both organs compared with the untreated control group. Co-administration of Fe-NPs plus EBEO succeeded to improve

Table 1. Details giving primer sequences for the genes amplified.

cDNA	Accession number	Forward primer	Reverse primer	RT-PCR product size	Reference
GAPDH	NM_017008.4	CAAGGTCATCCATGACAACTTTG	GTCCACCACCCTGTTGCTGTAG	496	Abdel-Wahhab et al. (2021)
Cu–Zn SOD	FQ210282.1	GCAGAAGGCAAGCGGTGAAC	TAGCAGGACAGCAGATGAGT	477	Limaye et al. (2003)
GPx	NM_030826.4	CTCTCCGCGGTGGCACAGT	CCACCACCGGGTCGGACATAC	290	Limaye et al. (2003)
CAT	NM_012520.2	GCGAATGGAGAGGCAGTGTAC	GAGTGACGTTGTCTTCATTAGCACTG	652	Gandhi et al. (2013)

Table 2. GC/MS analysis of the composition of basil essential oil.[a]

No	Identified compound[b]	%
1	Linalool	42.1
2	1,8-Cineole	7.8
3	(z)-isoeugeno	6.3
4	α-trans-bergamotene	4.9
5	1-epi-cubenol	4.6
6	(Z)-Anethole	3.8
7	trans-muurola-4-(14),5-diene	2.6
8	ϵ-Caryophyllene	2.3
9	isobornyl acetate	1.9
10	α-pinene	1.7
11	Aristolochene	1.6
12	cis-sabinene hydrate	1.3
13	1,10-di-epi-cubenol	1.3
14	Santolina triene	1.1
15	allo-aromadendrene	1.1
16	β-Ylangene	1.0
17	Spathulenol	1.0
18	β-pinene	1.0
19	cis-muurola-4-(14),5-diene	0.8
20	γ-muurolene	0.8
21	α-humulene	0.7
22	iso-isopulegol	0.7
23	trans-pulegol	0.7
24	β-copaene	0.6
25	α-gurjunene	0.6
26	γ-gurjunene	0.5
27	δ-cadinene	0.5
28	cis-β-elemenone	0.4
29	γ-himalachene	0.4
30	germacrene B	0.4
31	cis-calamenene	0.4
32	neo-isopulegol	0.4
33	Aromadendrene	0.4
34	iso-borneol	0.3
35	dehydro-sabina ketone	0.3
36	iso-3-thujanol	0.2
37	thuj-3-en-10-al	0.2
38	δ-elemene	0.2
39	trans-p-menth-6-en-2,8-diol	0.2
40	trans-cadina-1,4-diene	0.2
41	Terpinolene	0.1
42	p-Cymene	0.1
43	cis-muurol-5-en-4-β-ol	0.1
44	cis-dihydrocarvone	0.1
45	(6Z)-Nonenal	0.1
46	α-ylangene	0.1
47	10-epi-cubebol	0.1
48	neo-allo-ocimene	0.1

[a] Compound identified by GC/MS and/or by comparison of MS and LRI of standard compounds (ST) under the same conditions.

[b] The compounds are listed according to their concentration order, Linear retention index relative to n-alkanes (C7–C20) on DB-5 column.

these antioxidant enzymes in both tissues since the low dose could normalize renal CAT and the high dose could normalize hepatic and renal CAT and hepatic SOD.

To clarify these changes in the antioxidant enzymes, their relevant hepatic mRNA expression profile was examined using RT-qPCR (Figure 3). The results revealed that Fe-NPs induced a significant down-regulation in mRNA gene expression of GPx (Figure 3A), Cu–Zn SOD (Figure 3B) and CAT (Figure 3C) in hepatic tissues. EBEO alone did not induce any notable alterations in the expression of these genes. However, co-administration of EBEO plus Fe-NPs resulted in the up-regulation of mRNA expression and the declined expression was improved towards the level of the control group. Furthermore, no significant differences were noticed between the high or low-dose treated groups.

The present results showed that Fe-NPs increased significantly DNA fragmentation percentage (Table 8). However, insignificant difference was observed in DNA fragmentation of the normal control animals and those treated with EBEO. The co-treatment with EBEO (LD) or (HD) plus Fe-NPs reduced significantly the percent of DNA fragmentation compared with the Fe-NPs alone-treated group. The inhibition percent of DNA fragmentation reached 32.7 and 44.9% in the groups received the EBEO (LD) and (HD), respectively. As presented in Figure 4, the results of agarose gel electrophoresis of DNA confirmed the other results of colorimetric assays of DNA fragmentation and the antioxidant status, and corroborated the changed levels of the gene transcripts. The liver samples of rats administrated Fe-NPs showed a smear (hallmark of necrosis), DNA fragmentation without ladder formation, indicating random DNA degradation (Figure 4, Lane 2) compared with the control (Figure 4, Lane 1) and the EBEO-treated groups (Figure 4, Lanes 3 and 4). Treatment with EBEO at both dose levels markedly suppressed DNA fragmentation in rats received Fe-NPs (Figure 4, Lanes 5 and 6); where DNA was still localized at the starting point. Moreover, there was no significant difference between the DNA electrophoretic patterns of the EBEO-treated rats and the control groups.

The histological study of the liver in the untreated control group showed normal architecture with a classic hepatic lobule-containing central vein and radiating cords of hepatocytes with blood sinusoids in between, polyhedral hepatocytes with large and rounded vesicular nuclei. The blood sinusoids are presented between the cords of the hepatic cells and are lined by flattened endothelial and Kupffer cells (Figure 5A). The liver of animals in the Fe-NPs group showed hepatocytes vacuolar degeneration with pyknotic nuclei congested and enlarged portal vein and hyperplasia of the bile duct with periportal lymphocytic infiltration and fibrous tissues (Figure 5B). The liver of rats received EBEO (LD) showed normal hepatocytes around the central vein zone with remarkable hepatocellular vacuolar degeneration and nuclear pyknosis around the congested portal tract (Figure 5C). Moreover, the rats that received EBEO (HD) showed semi normal hepatocytes around the normal central vein a) and around the dilated and congested portal tract with hyperplasia in bile ducts lobules (Figure 5D). The examination of hepatic sections of rats treated with Fe-NPs plus EBEO (LD) showed no remarkable changes in hepatocytes and their blood vessels histological architecture (Figure 5E). Furthermore, the rats that received Fe-NPs plus EBEO (HD) showed marked improvement in hepatocytes histological architecture and a marked decrease in inflammatory cells (Figure 5F).

The examination of control kidney sections showed normal histology of glomeruli and proximal and distal convoluted tubules (Figure 6A). The kidney of rats exposed to Fe-NPs showed the different distribution of histological changes including necrosis in renal tubules and cellular debris in their lumen (N) and damaged glomeruli (D-G) interstitial dilation with inflammatory cellular and hemorrhagic spaces (Figure 6B). The kidney of rats received EBEO (LD) or EBEO (HD) showed a different distribution of histological structure where the renal tubules and glomeruli mesangial cells are nearly normal and interstitial spaces of inflammatory cells (Figure 6C). The kidney of the rats received Fe-NPs plus EBEO (LD) showed showing marked improvement in renal tubules and glomeruli cellularity (Figure 6D). The kidney of the rats in the Fe-NPs plus EBEO (HD) group showed a different distribution of nearly normal renal tubules and interstitial congestion and inflammatory cells (Figure 6E). Moreover, the same group showed deformed glomeruli with wide urinary spaces, shrinking in mesangial cells and some necrosis in

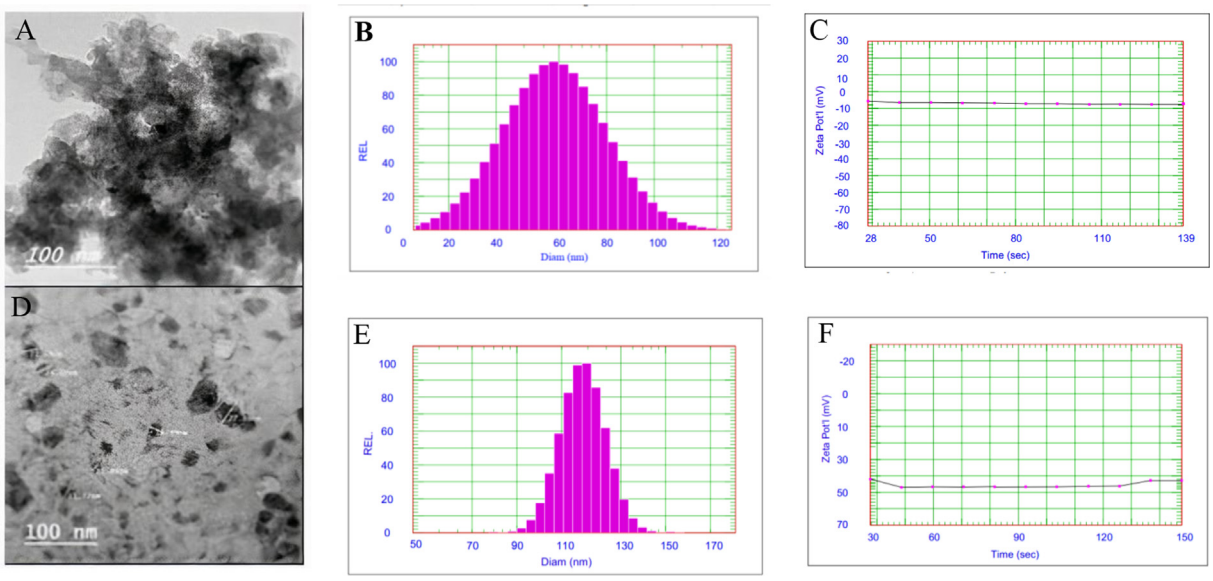

Figure 1. (A) TEM image of Fe-NPs showing the particle shape and size, (B) DLS analysis showing the size distribution of Fe-NPs, (C) ZetaSizer chromatogram showing the zeta potential of Fe-NPs, (D) TEM image of EBEO showing the particle shape and size (E) DLS analysis showing particles distribution of EBEO, and (F) ZetaSizer chromatogram showing the zeta potential of EBEO.

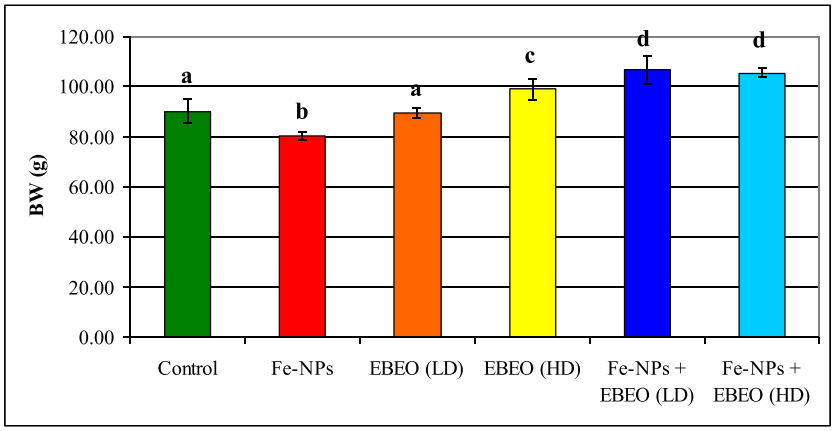

Figure 2. Effect of EBEO on body weight in animals treated with Fe-NPs.

Table 3. Effects of EBEO on serum biochemical parameters in rats treated with Fe-NPs.

Parameter Groups	ALT (U/L)	AST (U/L)	TP (g/dl)	Creatinine (mg/dl)	Urea (mg/dl)
Control	49.16 ± 4.23^{a}	163.53 ± 6.04^{a}	8.33 ± 0.41^{a}	0.47 ± 0.03^{a}	30.33 ± 0.67^{a}
Fe -NPs	153.67 ± 6.53^{b}	187.45 ± 5.86^{b}	6.32 ± 0.27^{b}	0.77 ± 0.03^{b}	38.67 ± 1.20^{b}
EBEO (LD)	47.95 ± 3.63^{a}	162.07 ± 3.44^{a}	8.77 ± 0.13^{a}	0.50 ± 0.01^{a}	31.33 ± 0.67^{a}
EBEO (HD)	48.95 ± 5.93^{a}	164.25 ± 2.89^{a}	8.27 ± 0.18^{a}	0.50 ± 0.06^{a}	32.33 ± 1.45^{a}
Fe-NPs + EBEO (LD)	58.58 ± 6.06^{c}	180.60 ± 9.18^{c}	7.64 ± 0.25^{c}	0.51 ± 0.03^{a}	34.67 ± 0.67^{c}
Fe-NPs + EBEO (HD)	48.8 1 ± 1.35^{a}	164.91 ± 5.98^{a}	8.38 ± 0.23^{a}	0.47 ± 0.03^{a}	29.80 ± 0.58^{a}

Within each column, means superscripts with different letters are significantly different ($P < 0.05$).

the renal tubular epithelium, focal congestion and inflammation, and some tubules epithelial cells were damaged (Figure 6F).

4. Discussion

The GC-MS analysis of BEO showed the isolation of 48 compounds and Linalool, 1,8-Cineole, (z)-isoeugeno, α-trans-bergamotene, 1-epi-cubenol, (Z)-Anethole, trans-muurola-4-(14),5-diene and €-Car-yophyllene besides some other compounds were found in a concentration less than 2%. These results are similar to the recent report by Amor et al. (2021) and Benedec et al. (2013) who showed that linalool was the major compound in BEO. However, Olugbade et al. (2017) reported that methyl eugenol was the major compound followed by methyl chavicol and Ghasemi Pirbalouti et al. (2017) reported that methyl chavicol is the

Table 4. Effects of EBEO on lipid profile parameters in rats treated with Fe-NPs.

Parameter Groups	Cholesterol (mg/dl)	TG (mg/dl)	HDL (mg/dl)	LDL (mg/dl)
Control	62.35 ± 4.39[a]	28.32 ± 3.0[a]	31.33 ± 0.33[a]	47.71 ± 1.88[a]
Fe -NPs	87.98 ± 1.96[b]	34.52 ± 3.86[b]	23.73 ± 0.92[b]	66.13 ± 1.90[b]
EBEO (LD)	63.34 ± 1.29[a]	26.78 ± 1.97[a]	44.90 ± 2.35[c]	46.64 ± 1.06[a]
EBEO (HD)	61.87 ± 1.4[a]	26.57 ± 2.20[a]	53.15 ± 1.45[d]	48.85 ± 0.75[a]
Fe-NPs + EBEO (LD)	76.63 ± 2.16[a]	24.94 ± 2.30[c]	30.47 ± 0.50[a]	46.72 ± 0.95[a]
Fe-NPs + EBEO (HD)	72.77 ± 3.80[a]	28.33 ± 1.83[a]	32.01 ± 2.91[a]	47.22 ± 1.12[a]

Within each column, means superscripts with different letters are significantly different ($P < 0.05$).

Table 5. Effects of EBEO on tumor markers in rats treated with Fe-NPs.

Parameter Groups	AFP (ng/ml)	TNF-α (ng/ml)	CEA (ng/ml)
Control	0.02 ± 0.01[a]	0.30 ± 0.04[a]	2.57 ± 0.23[a]
Fe-NPs	0.42 ± 0.01[b]	0.42 ± 0.04[b]	4.77 ± 0.26[b]
EBEO (LD)	0.02 ± 0.01[a]	0.31 ± 0.02[a]	2.23 ± 0.15[a]
EBEO (HD)	0.02 ± 0.01[a]	0.31 ± 0.01[a]	2.63 ± 0.22[a]
Fe-NPs + EBEO (LD)	0.28 ± 0.03[c]	0.33 ± 0.01[c]	3.30 ± 0.12[c]
Fe-NPs + EBEO (HD)	0.06 ± 0.02[d]	0.31 ± 0.01[a]	2.25 ± 0.21[a]

Within each column, means superscripts with different letters are significantly different ($P < 0.05$).

Table 6. Effects of EBEO on hepatic and real No and MDA in rats treated with Fe-NPs.

Parameter Groups	NO (μmol/g tissue)		MDA (nmol/g tissue)	
	Liver	Kidney	Liver	Kidney
Control	2.01 ± 0.15[a]	1.99 ± 0.07[a]	44.87 ± 2.07[a]	92.48 ± 1.69[a]
Fe -NPs	6.01 ± 0.40[b]	3.54 ± 0.25[b]	78.84 ± 2.42[b]	145.51 ± 13.16[b]
EBEO (LD)	2.03 ± 0.05[a]	2.26 ± 0.20[c]	43.63 ± 1.50[a]	101.27 ± 2.22[a]
EBEO (HD)	2.02 ± 0.40[a]	2.21 ± 0.18[c]	44.46 ± 2.40[a]	104.96 ± 2.46[a]
Fe-NPs + EBEO (LD)	3.13 ± 0.09[c]	2.12 ± 0.07[a]	46.07 ± 1.89[a]	85.34 ± 2.35[c]
Fe-NPs + EBEO (HD)	2.05 ± 0.12[a]	2.02 ± 0.10[a]	42.44 ± 2.20[a]	84.23 ± 1.36[c]

Within each column for each organ, means superscripts with different letters are significantly different ($P < 0.05$).

Table 7. Effects of EBEO on hepatic and renal antioxidant enzymes in rats treated with Fe-NPs.

Parameter Groups	GPx (U/g)		CAT (mU/g)		SOD (U/g)	
	Liver	Kidney	Liver	Kidney	Liver	Kidney
Control	320.78 ± 2.21[a]	219.00 ± 0.88[a]	9.44 ± 0.05[a]	9.68 ± 0.08[a]	36.77 ± 0.90[a]	34.79 ± 2.37[a]
Fe -NPs	128.28 ± 2.95[b]	111.47 ± 0.14[b]	6.38 ± 0.27[b]	7.55 ± 0.13[b]	21.91 ± 1.28[b]	14.64 ± 1.84[b]
EBEO (LD)	326.27 ± 3.48[a]	218.71 ± 1.68[a]	9.52 ± 0.13[a]	9.40 ± 0.14[a]	37.43 ± 1.56[a]	39.01 ± 0.32[a]
EBEO (HD)	331.96 ± 1.30[c]	222.59 ± 1.76[a]	10.79 ± 0.10[c]	9.56 ± 0.05[a]	42.89 ± 0.79[c]	39.14 ± 1.20[c]
Fe-NPs + EBEO (LD)	216.76 ± 3.54[d]	144.79 ± 0.66[c]	8.18 ± 0.29[d]	9.22 ± 0.01[a]	29.26 ± 1.95[d]	24.84 ± 0.54[d]
Fe-NPs + EBEO (HD)	219.46 ± 2.58[d]	147.54 ± 0.07[c]	9.01 ± 0.06[a]	9.31 ± 0.04[a]	36.54 ± 0.77[a]	27.68 ± 0.52[d]

Within each column, means superscripts with different letters are significantly different ($P < 0.05$).

major compound followed by linalool. The percentage of the major components varied according to geographical origin (Ahmed et al., 2019; Diniz do Nascimento et al., 2020).

The synthesized EBEO showed a smooth round shape with an average particle size of 120 nm and a zeta potential of -6.4 mV suggesting that WPI enhanced the droplet coalescence (Goula and Adamopoulos, 2012). Moreover, the uniform size distribution of oil droplets and the smooth round shape indicated the formation of a droplet wall material by WPI (Noello et al., 2016; Eratte et al., 2014). A previous study reported that the shape, surface property and size of the nanoparticles have a pivotal role in the uptake of nanosized particles by the cells and the size between 50-300 nm has a favorable uptake than the counterparts (Roger et al., 2010). Besides, the size of nanoparticles affects the distribution, clearance and pharmacokinetics (Sadat et al., 2016). Furthermore, zeta potential plays an important role in the distribution of the droplets and increases their stability (McClements and Rao, 2011). The -ve zeta potential reported herein for the NEBO is attributed to the negative charge of carboxylate groups in WPI which is the only functional charge in the globulars of WPI (Eratte et al., 2014). Further, the addition of basil leaves extracts to $FeSO_4$ resulted in the synthesis of Fe-NPs. This indicated that

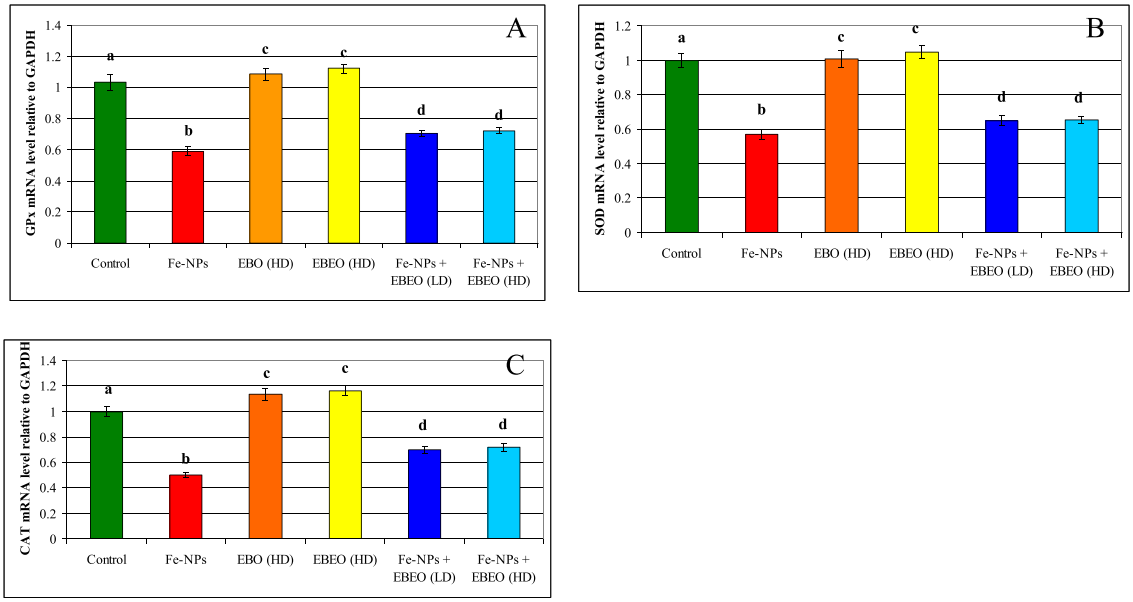

Figure 3. Effect of EBEO on relative expression of (A) GPx, (B) SOD and (C) CAT gene in liver of rats treated with Fe-NPs. Analyses were performed in triplicate. Data are the mean ± SE of three different liver samples in same group. Means within columns carrying different superscript letters are significantly different at $P \leq 0.05$.

Table 8. Effect of EBEO on DNA fragmentation in the liver of rats treated with Fe-NPs.

Treatment	DNA fragmentation %	DNA fragmentation inhibition %
Control	9.8 ± 0.1^{a}	
Fe -NPs	24.5 ± 0.76^{c}	
EBEO (LD)	10.4 ± 0.31^{a}	
EBEO (HD)	9.6 ± 0.35^{a}	
Fe-NPs + EBEO (LD)	16.5 ± 0.61^{b}	32.7
Fe-NPs + EBEO (HD)	13.5 ± 0.87^{b}	44.9

Means superscripts with different letters are significantly different ($P < 0.05$).

basil leaves extract acted as a reducing agent in the synthesis process of Fe-NPs. In previous work, Hafiz et al. (2018) synthesized different shapes of Fe-NPs e.g. spikes, rod shape, spherical and cube using the extract of *Spinacia oleracea* leaves with particle size range from 100-205 nm. The variation in size and morphology of nanoparticles synthesized from different metal ions using plant extracts significantly affect their electronic, chemical and physical properties (Khan et al., 2019). The formation of Fe-NPs in the current study may be due to the ability of different metabolites in the basil extract including the polyphenols, terpenoids, alkaloids, sugars, proteins and phenolic acids which play a vital role in the bioreduction of the metal ions resulting in heterogeneous shapes and sizes of nanoparticles (Bibi et al., 2019; Fahmy et al., 2018; Hafiz et al., 2018). The zeta potential value reported herein for Fe-NPs was 42.42 mV suggested that the synthesized Fe-NPs are stable. In this concern, previous reports revealed that zeta potential over 60 mV indicates excellent stability, zeta potential above 30 mV and below 20 mV indicate physical and limited stability, respectively; however, zeta potential lower than 5 mV are the index of agglomeration (Mahbubul, 2019).

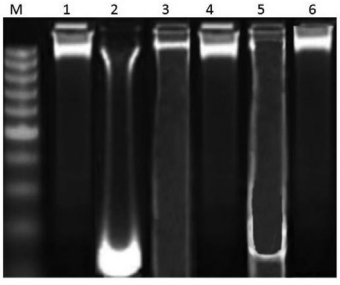

Figure 4. Agarose gel electrophoresis of extracted DNA from liver of rats treated with Fe-NPs alone or plus EBEO at low and high dose. These results confirmed that treatment with EBEO attenuates Fe-NPs-induced hepatotoxicity in rats. Lane M, 100 bpDNA ladder; Lane 1 untreated control group; Lane2, Fe-NPs-treated group; Lane3, EBEO (LD)-treated group, lane 4, EBEO (HD); Lane 5, EBEO (LD) plus Fe-NPs-treated group and lane 6, EBEO (HD) plus Fe-NPs-treated group.

In this investigation, we evaluated the effect of subchronic oral administration of Fe-NPs on liver and kidney and the possible protective role of EBEO in rats. The selected dose of Fe-NPs and EBEO were based on the literature (Kulkarni et al., 2020; Yacout et al., 2012, respectively). Our results showed that treatment with Fe-NPs induced significant effects on body weight, liver and kidney parameters, serum cytokines, lipid profile accompanied by an elevation of oxidative markers and the decrease of antioxidant enzyme activity in the liver and kidney.

Administration of Fe-NPs increased in ALT, AST, and decreased the level of TP. The elevated in these enzymes suggested that Fe-NPs cause hepatic injury or necrosis (Nasrin et al., 2018) and altered the permeability of the hepatocellular membrane (Mohamed et al., 2015; Ates et al., 2016). In this concern, Sadauskas et al. (2007) and Bao et al. (2015) demonstrated that Fe-NPs are taken up by the hepatocytes and Kupffer cells (specialized macrophages located in the liver). Fe-NPs are degraded Fe^{+2} and Fe^{+3} products that are incorporated into the storage or utilization pathways (e.g. hemoglobin, ferritin, and transferrin). In contrast, Parivar et al. (2016) reported that oral administration of Fe-NP significantly reduced the activity of ALT, AST, and LDH. Taken together, the obtained data imply that conventional serum biochemical assessments should be cautiously used in safety evaluations of NMs (Garcia--Fernandez et al., 2020).

Creatinine and urea are the indices for renal function and they increase during kidney dysfunction. The increase in kidney indices in the Fe-NPs-treated group proposed that these particles affect the filtration rate of the glomerular and the ability of the kidney to induce blood filtration (Du et al., 2018; Mohammed et al., 2020). Moreover, the decreased level of total protein suggested liver necrosis and/or protein

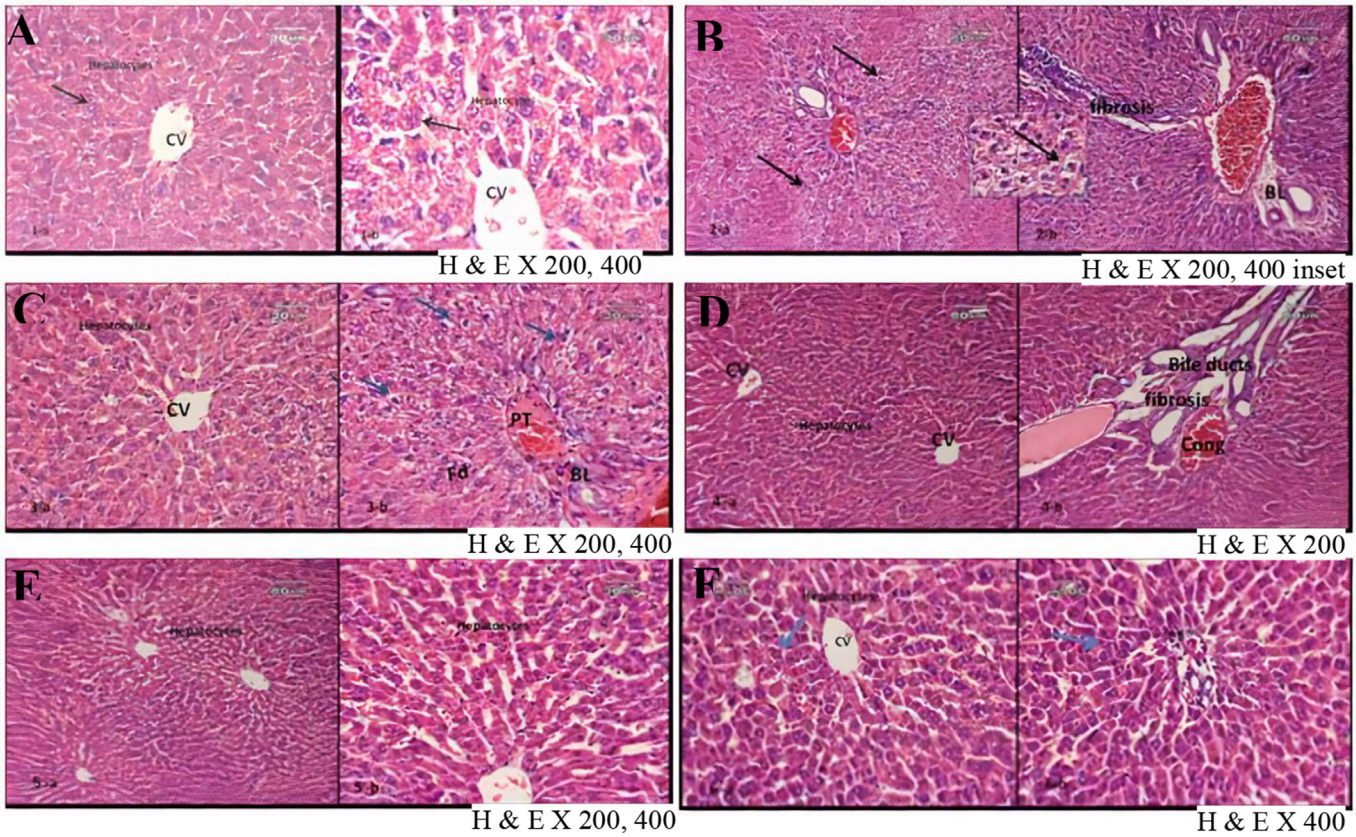

Figure 5. Photomicrographs of liver sections of: (A) control group showing normal liver architecture, a classic hepatic lobule-containing central vein (cv) and radiating cords of hepatocytes with blood sinusoids in between (arrow), polyhedral hepatocytes with large, rounded vesicular nuclei (arrow), blood sinusoids (s) are present in between the cords of hepatocytes and are lined by flattened endothelial cells and Kupffer cells; (B) rats treated with Fe-NPs showing hepatocytes vacular degeneration with pyknotic nuclei (arrow & inset), congested and enlarged portal vein (CG) and hyperplasia of bile duct (BL) with periportal lymphocytic infiltration and fibrous tissues; (C) rats treated with EBEO(LD) showing (a) normal hepatocytes around the central vein zone while remarkable hepatocelular vacuolar degeneration and nuclear pyknosis around the congested portal tract are seen; (D) rats treated with EBEO (HD) showing nearly normal hepatocytes around the normal central vein and around the dilated and congested portal tract with a hyperplasia in bile ducts lobules; (E) rats treated with Fe-NPs plus EBEO(LD) showing no remarkable changes in hepatocytes and their blood vessels with normal histological architecture and (F) rats treated with Fe-NPs plus EBEO(HD) showing marked improvement in hepatocytes histological architecture and marked decrease in inflammatory cells.

catabolism escort kidney dysfunction (Abdel-Wahhab et al., 2007; Parivar et al., 2016; Nasrin et al., 2018). Treatment with Fe-NPs increased cholesterol, TG, LDL, and decreased HDL suggesting dyslipidemia. Dyslipidemia is considered a high-risk factor for coronary heart diseases (Litvinov et al., 2012). Consequently, the present results suggested that Fe-NPs are probably responsible for the disturbances in the lipid metabolism and atherosclerosis with cardiovascular disease risk (Litvinov et al., 2012). In this concern, Nemmar et al. (2016) reported that Fe-NPs increase CK-MB levels in the heart and plasma tissues. Also, Shen et al. (2015) demonstrated that Fe-NPs attack the myocardium muscles inducing myocardial iron overload, resulting in myocardial injury and deterioration of cardiac function (Nasrin et al., 2018).

The reduction in GPx, CAT, and SOD and their mRNA gene expression in hepatic and renal tissue of rats after Fe-NPs administration and the elevation of MDA and NO indicated the occurrence of oxidative damage in both liver and kidney. According to Zhu et al. (2017), MDA is the main degradation product of the peroxidation of lipid; whereas, NO is critical free radical which induces severe damage to cells when produced excessively in the tissues or serum (Birben et al., 2015). Therefore, the oxidative damage of Fe-NPs may lead to enzymatic degradation in lysosome due to high acidic environment and release Fe^{+2} which react with H_2O_2 in mitochondria induces production of ROS such as hydroxyl particles through Fenton reaction (Chen 2019; Toyokuni, 2009). Moreover, ROS lead to mitochondrial damage, lipid peroxidation, or protein oxidation, which can then induce a cascade of Ca^2-dependent signaling mechanisms resulting in cell death (Soenen et al., 2012).

One of the principal mechanisms of Fe-NPs-induced toxicity is the generation of ROS that resulted in oxidative stress. Oxidative stress is the subsequent production of inflammatory mediators and DNA damage (Helm and Rudel, 2020). In this concern, Toyokuni (2009) suggested that Fe-NPs increase ROS, MDA and decrease GPx, SOD, and CAT and their mRNA expression as a mechanism of liver damage. Moreover, Fe-NPs caused membrane damage, leakage of lactate dehydrogenase, reduction in SOD, and CAT activity (Hasanuzzaman et al., 2020). These results agree with the previous study of Arbab et al. (2005). Taken together, the decreased of antioxidants levels and the increased MDA and NO levels confirmed that Fe-NPs induce the generation of ROS which include hydrogen peroxide, hydroxyl radicals, and superoxide anions, thus causing oxidative stress and disrupt the antioxidant system, resulting in membrane lipid peroxidation, oxidation of the enzymes and structural proteins, DNA damage, and cell death (Toyokuni, 2009; Singh et al., 2010). Additionally, Rim et al. (2013) and Yousef et al. (2019) reported that nanoparticles induce oxidative DNA damage not only through corrosion and the release of metal ions, but also as a result of chronic inflammatory responses.

The current results also showed that Fe-NPs administration increased the serum AFP, TNF-α, and CEA suggested the disturbance of the immune system. Previous reports revealed that macrophages are the most AFP,

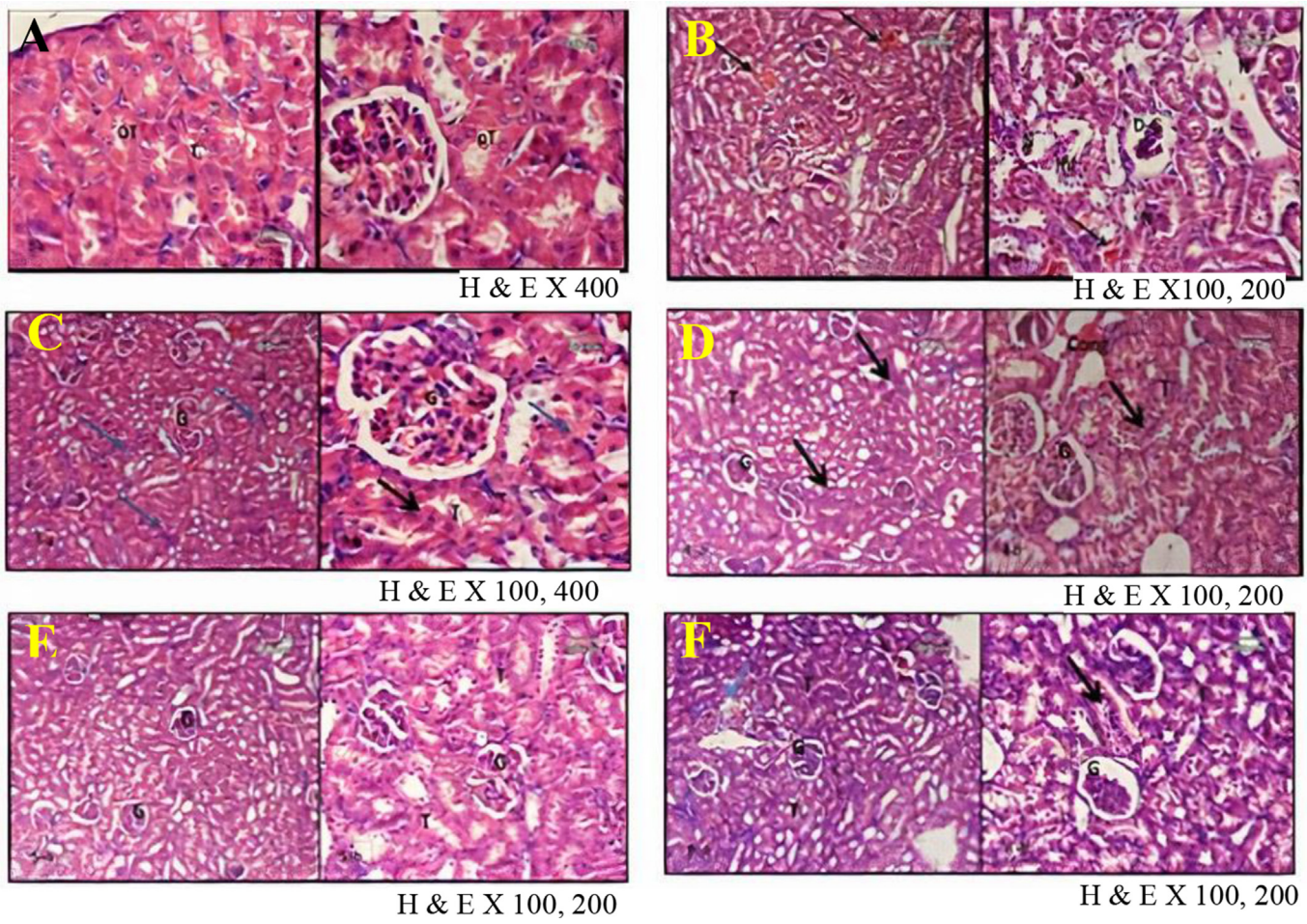

Figure 6. Photomicrograph of kidney sections of (A) control rats showing normal histology of glomeruli (F), renal tubules proximal (PT) and distal (DT) convoluted tubules; (B) rats treated with Fe-NPs showing different distribution of histological changes in the form of necrosis in renal tubules and cellular debris in their lumen (N) and damaged glomeruli (D–F) interstitial dilation with inflammatory cellular and haemohrrageic spaces (arrow); (C) rats treated with EBEO (LD) showing different distribution of histological structure where the renal tubules and glomeruli mesangial cells are nearly normal with interstitial spaces of inflammatory cells (arrow); (D) rats treated with EBEO (HD) showing different distribution of nearly normal renal tubules and interstitial congestion and inflammatory cells also seen (arrow); (E) rats treated with Fe-NPs plus EBEO (LD) showing marked improvement in renal tubules and glomeruli cellularity, and (E) rats treated with Fe-NPs plus EBEO (HD) showing deformed glomeruli with wide urinary spaces, shrinking in mesangial cells and some necrosis in renal tubular epithelium (F). Focal congestion and inflammation, some tubule s epithelial cells are damaged (arrow).

TNF-α, and CEA producers and these markers are playing a critical role in tumor conditions (Aldubayan et al., 2019). TNF-α is an important factor in the promotion of tumors (Choi et al., 2010). It is also considered a key factor in the regulation of several cytokines production responsible for the chronic inflammation and the development of tumor via the NF-kB pathway (Karabela et al., 2011). Generally, the increased level of MDA, NO, AFP, TNF-α, and CEA and the decreased in GPx, CAT and SOD and their corresponding gene expression revealed that the toxicity of Fe-NPs is mainly via the production of ROS and inflammation (Reddy et al., 2017; Soenen et al., 2012).

Another mechanism of Fe-NPs-induced toxicity is the accumulation of these particles in the cytoplasm leading to damage of mitochondria, disruption in ATP synthesis, and Ca^{2+} buffering. When the iron entrance to the mitochondria, it is used in heme and Fe–S cluster synthesis or stored by mitochondrial ferritin. Excess Fe^{+2} in the mitochondria altered the permeability causing Ca^{2+} and cytochrome C release into the cytoplasm and result in apoptosis activation (Sripetchwandee et al., 2016). Moreover, the increase of free iron concentration within the cell stimulates OH production via the Fenton-like reaction due to mobilization of Fe^{2+} by Ca^{2+} resulting in further cell damage suggesting other mechanisms of Fe-NPs toxicity (Malvindi et al., 2014). The histological study of liver and kidney sections in rats in the Fe-NPs group showed severe histological changes typical to those reported in the previous studies (Talesh et al., 2019). These findings confirmed the biochemical results of the current study and supported that Fe-NPs administration induced hepato-nephrotoxicity mainly through the generation of oxidative damage and the immunodeficiency response.

Several reports demonstrated that the main constituents of *O. basilicum* essential oil were linalool and the methyl chavicol (Avetisyan et al., 2017; Theodosiou et al., 2014). Previously, the protective role of linalool against oxidative DNA damage has been evaluated with alkaline Comet assay on *S. cerevisiae* (Nikolić et al., 2019). Encapsulation as a promising technique manages a controlled release and boosted the stability and bioavailability of bioactive compounds/drugs (Liang et al., 2012; Donsi et al., 2012). Animals treated with EBEO alone at both dose levels were comparable with the control however, the combined treatments with Fe-NPs plus EBEO showed a protective against Fe-NPs toxicity. Most of the tested parameters showed significant improvement towards the control values and the high dose was more effective. Similar results were stated by Rafael et al. (2018), Ahmed et al. (2019) who showed the higher antioxidant property of linalool. Moreover, linalool act as pro-oxidants and induce DNA strand breaks (Tamoghna et al., 2018) and decreased ROS production.

Huo et al. (2013) showed that linalool reduces the production of IL-6 and TNF-α induced by LPS in *vitro and in vivo*; block phosphorylation of IkBa protein, c-Jun terminal kinase, p38 and extracellular signal-regulated kinase. Moreover, another study suggested that it's beneficial for the treatment of kidney damage in diabetic subjects through the attenuation of TGF-b1 and NF-kB expression (Deepa and Venkatraman Anuradha, 2013). Additionally, linalool act on inflammatory by preventing pro-inflammatory factors secretion via the decrease of lipopolysaccharide (LPS)/D-galactosamine (GalN)-induced liver injury in mice through inhibition of the expression of caspase-8 and caspase-3 and the elimination of inflammatory response via NF-kB suppression (Li et al., 2014; De Andrade et al., 2017).

Moreover, the Cis-verbenol another phytochemical constituent of the essential oil of *O. basilicum* has been anti-inflammatory property via the suppression of pro-inflammatory cytokines expression levels in the ischemic brain and immune stimulated glial cells (Rashidian et al., 2016). Also, phenolic thymol and Cis-verbenol were found to induce the high antioxidative effect of LDL and decrease plasma levels of TG and cholesterol with no adverse effects in kidneys or liver (Ebenyi et al., 2012). These compounds also are important free radicals scavengers' natural products and possess antioxidant properties (Ebenyi et al., 2012). In addition, EBEO increases the levels of other natural antioxidants in the body, such as SOD and CAT which protect the liver from PAR-induced hepatotoxicity (El-Banna et al., 2013). The mechanisms postulated to BEO as antioxidants including (1) scavenging of ROS; (2) chelation of iron which initiates radical reactions and inhibition of enzymes responsible for the generation of ROS (Edenharder and Gruñhage, 2003); (3) antioxidants can interfere with xenobiotic-metabolizing enzymes, block activated mutagens/carcinogens, modulate DNA repair and even regulate gene expression (Paramasivan et al., 2019). All these mechanisms may be important for their antimutagenic and anticarcinogenic properties (De Flora and Ferguson, 2005). In the present study, whey protein (WP) was used as wall material in the encapsulation of the essential oil; hence, we can suggest another mechanism for EBEO-induced protection. WP is a well-known antioxidant and hepatoprotective agent (Gad et al., 2011) due to its high content of amino acids cysteine, α-lactoglobulin, bovine serum albumin, and β-lactoglobulin (Minj and Anand, 2020). Generally, the protective and antimutagenic activity of EBEO is mainly attributed to the antioxidative properties of different phenolic components in the oil.

5. Conclusion

The present work indicated that spherical shape Fe-NPs with an average particle size of 60 ± 4.76 nm and zeta potential of 42.42 mV can be synthesized by green chemistry using basil leave extract. The encapsulated basin essential oil using WPI resulted in an average capsule size of 120 ± 3.2 nm and a zeta potential of -6.4 mV. The GC-Ms data revealed the identification of 48 compounds in the basin essential oil and the major compounds were Linalool, 1,8-Cineole, (z)-isoeugeno, α-trans-bergamotene, 1-epi-cubenol, (Z)-Anethole, trans-muurola-4-(14),5-dieneand €-Caryophyllene. The *in vivo* results showed that Fe-NPs induced significant toxic effects as manifested by the alterations in the biochemical parameters related to liver and kidney function. Fe-NPs increased oxidative damage markers, cytokines and decreased the activity of antioxidant enzymes and their corresponding gene expression and induced histological alterations in liver and kidney. Additionally, these particles increased the hepatic DNA fragmentation. EBEO did not induce any notable changes although it enhances the antioxidant capacity, especially at the high dose. EBEO could mitigate Fe-NPs toxicity and the higher dose succeeded to normalize almost all the tested parameters. The current results concluded that EBEO is a promising agent can be used safely in food or pharmaceutical application for the protection against Fe-NPs.

Declarations

Author contribution statement

Aziza A. El-Nekeety; Marwa E Hassan; Rasha R. Hassan; Ola I Elshafey; Zeinab K. Hamza; Sekena H. Abdel-Aziem; Nabila S. Hassan: Performed the experiments; Analyzed and interpreted the data; Contributed reagents, materials, analysis tools or data.

Mosaad A. Abdel-Wahhab: Conceived and designed the experiments; Wrote the paper.

Funding statement

This work was supported by the National Research Centre, Dokki, Cairo, Egypt project #12050305.

Data availability statement

Data will be made available on request.

Declaration of interests statement

The authors declare no conflict of interest.

Additional information

No additional information is available for this paper.

References

Abdel-Wahhab, M.A., Abdel-Galil, M.M., Hassan, A.M., Hassan, N.H., Nada, S.A., Saeed, A., El-Sayed, M.M., 2007. *Zizyphus spina-christi* extract protects against aflatoxin B_1-intitiated hepatic carcinogenicity. Afr. J. Trad. CAM. 4 (3), 248–256.

Abdel-Wahhab, M.A., Aljawish, A., El-Nekeety, A.A., Abdel-Aziem, S.H., Hassan, N.S., 2017. Chitosan nanoparticles plus quercetin suppress the oxidative stress, modulate DNA fragmentation and gene expression in the kidney of rats fed ochratoxin A-contaminated diet. Food Chem. Toxicol. 99, 209–221.

Abdel-Wahhab, M.A., El-Nekeety, A.A., Hassan, N.S., Gibriel, A.A., Abdel-Wahhab, K.G., 2018. Encapsulation of cinnamon essential oil in whey protein enhances the protective effect against single or combined sub-chronic toxicity of fumonisin B_1 and/or aflatoxin B_1 in rats. Environ. Sci. Pollu. Res. 25 (29), 29144–29161.

Abdel-Wahhab, M.A., El-Nekeety, A.A., Mohammed, H.E., Elshafey, O.I., Abdel-Aziem, S.H., Hassan, N.S., 2021. Elimination of oxidative stress and genotoxicity of biosynthesized titanium dioxide nanoparticles in rats via supplementation with whey protein-coated thyme essential oil. Environ. Sci. Pollut. Res. Int.

Adams, R.B., 2007. Identification of essential oil components by gas chromatography/quadruple mass spectroscopy. Carol Stream. Allured publishing Co, IL, USA.

Aguilar-Veloz, L.M., Calderón-Santoyo, M., González, Y.V., Ragazzo-Sánchez, J.A., 2020. Application of essential oils and polyphenols as natural antimicrobial agents in postharvest treatments: advances and challenges. Food Sci. Nutr. 8, 2555–2568.

Ahmed, A.F., Attia, F.A.K., Liu, Z., Li, C., Wei, J., Wenyi, Kang, W., 2019. Antioxidant activity and total phenolic content of essential oils and extracts of sweet basil (*Ocimum basilicum* L.) plants. Food Sci. Hum. Well 8 (3), 299–305.

Ajinkya, N., Yu, X., Kaithal, P., Luo, H., Somani, P., Ramakrishna, S., 2020. Magnetic iron oxide nanoparticle (IONP) synthesis to applications: present and future. Materials 13 (20), 4644.

Aldubayan, M.A., Elgharabawy, R.M., Ahmed, A.S., Tousson, E., 2019. Antineoplastic activity and curative role of avenanthramides against the growth of Ehrlich solid tumors in mice. Oxid. Med. Cell Long. Article ID 5162687.

Alsaraf, S., Hadi, Z., Al-Lawati, W.M., Al Lawati, A.A., Khan, S.A., 2020. Chemical composition, *in vitro* antibacterial and antioxidant potential of Omani Thyme essential oil along with in silico studies of its major constituent. J King Saud Univ Sci 32 (1), 1021–1028.

Amor, G., Sabbah, M., Caputo, L., Idbella, M., De Feo, V., Porta, R., Fechtali, T., Mauriello, G., 2021. Basil essential oil: composition, antimicrobial properties and microencapsulation to produce active chitosan films for food packaging. Foods 10 (1), 121.

Arbab, A.S., Wilson, L.B., Ashari, P., Jordan, E.K., Lewis, B.K., Frank, J.A., 2005. A model of lysosomal metabolism of dextran coated super paramagnetic iron oxide (spio) nanoparticles: implications for cellular magnetic resonance imaging. NMR Biomed. 18 (6), 383–389.

Ates, M., Demir, V., Arslan, Z., Kaya, H., Yilmaz, S., Camas, M., 2016. Chronic exposure of tilapia (*Oreochromis niloticus*) to iron oxide nanoparticles: effects of particle morphology on accumulation, elimination, hematology and immune responses. Aquat. Toxicol. 177, 22–32.

Avetisyan, A., Markosian, A., Petrosyan, M., Sahakyan, N., Babayan, A., Aloyan, S., Trchounian, A., 2017. Chemical composition and some biological activities of the

essential oils from basil Ocimum different cultivars. BMC Compl. Alternative Med. 17, 60.
Bancroft, D., Stevens, A., Turmer, R., 1996. Theory and Practice of Histological Technique, fourth ed. Churchill Livingstone, Edinburgh, pp. 36–42.
Bao, Y., Wen, T., Samia, A.C.S., Khandhar, A., Krishnan, K.M., 2015. Magnetic nanoparticles: material engineering and emerging applications in lithography and biomedicine. J. Mater. Sci. 51, 513–553.
Benedec, D., Oniga, I., Toiu, A., Tiperciuc, B., Tămaş, M., Vârban, I.D., Crişan, G., 2013. GC-MS analysis of the essential oil obtained from *ocimum basilicum* L."holland" cultivar. FARMACIA 61 (3), 448–453.
Bibi, I., Nazar, N., Ata, S., Sultan, M., Ali, A., Abbas, A., Jilani, K., Kamal, S., Sarim, F.M., Khan, M.I., Jalal, F., Iqbal, M., 2019. Green synthesis of iron oxide nanoparticles using pomegranate seeds extract and photocatalytic activity evaluation for the degradation of textile dye. J. Mater. Res. Technol. 8 (6), 6115–6124.
Birben, E., Sahiner, U.M., Sackesen, C., Erzurum, S., Kalayci, O., 2015. Oxidative stress and antioxidant defense. World Allergy Organ J. 5 (1), 9–19.
Chen, H.Y., 2019. Why the reactive oxygen species of the Fenton reaction switches from oxoiron (IV) species to hydroxyl radical in phosphate buffer solutions? a computational rationale. ACS Omega 4 (9), 14105–14113.
Chitprasert, P., Sutaphanit, P., 2014. Holy basil (*Ocimum sanctum* Linn.) essential oil delivery to swine gastrointestinal tract using gelatin microcapsules coated with aluminum carboxymethyl cellulose and beeswax. J. Agric. Food Chem. 62, 12641–12648.
Choi, I.Y., Lim, J.H., Hwang, S., Lee, J.C., Cho, G.S., Kim, W.K., 2010. Antiischemic and anti-inflammatory activity of (S)-cis-verbenol. Free Radic. Res. 44, 541–551.
Dadfar, S.M., Roemhild, K., Drude, N.I., von Stillfried, S., Knüchel, R., Kiessling, F., Lammers, T., 2019. Iron oxide nanoparticles: diagnostic, therapeutic and theranostic applications. Adv. Drug Deliv. Rev. 138, 302–325.
Dawood, M., El Basuini, M.F., Zaineldin, A.I., Yilmaz, S., Hasan, M.T., Ahmadifar, E., El Asely, A.M., Abdel-Latif, H., Alagawany, M., Abu-Elala, N.M., Van Doan, H., Sewilam, H., 2021. Antiparasitic and antibacterial functionality of essential oils: an alternative approach for sustainable aquaculture. Pathogens 10 (2), 185.
De Andrade, C.J., Andrade, L.R., Silvana, S.M., Pastore, G., Jauregi, P., 2017. A novel approach for the production and purification of mannosylerythritol lipids (MEL) by *Pseudozyma tsukubaensis* using cassava wastewater as substrate. Separ. Purif. Technol. 180, 157–167.
De Flora, S., Ferguson, R.L., 2005. Overview of mechanisms of cancer chemopreventive agents. Mutat. Res. 591, 8–15.
Deepa, B., Venkatraman Anuradha, C., 2013. Effects of linalool on inflammation, matrix accumulation and podocyte loss in kidney of streptozotocin-induced diabetic rats. Toxicol. Mech. Methods 23, 223–234.
Diniz do Nascimento, L., Moraes, A.A.B., Costa, K.S.D., Pereira Galúcio, J.M., Taube, P.S., Costa, C.M.L., Neves Cruz, J., de Aguiar Andrade, E.H., Faria, L.J.G., 2020. Bioactive natural compounds and antioxidant activity of essential oils from spice plants: new findings and potential applications. Biomolecules 10 (7), 988.
Dönmez Güngüneş, Ç., Şeker, Ş., Elçin, A.E., Elçin, Y.M., 2017. A comparative study on the *in vitro* cytotoxic responses of two mammalian cell types to fullerenes, carbon nanotubes and iron oxide nanoparticles. Drug Chem. Toxicol. 40 (2), 215–227.
Donsi, F., Annunziata, M., Vincensi, M., Ferrari, G., 2012. Design of nanoemulsion-based delivery systems of natural antimicrobials: effect of the emulsifier. J. Biotechnol. 159, 342–350.
Du, B., Mengxiao, Y., Jie, Z., 2018. Transport and interactions of nanoparticles in the kidneys. Nat. Rev. Mater. 3.
Ebani, V.V., Nardoni, S., Bertelloni, F., Pistelli, L., Mancianti, F., 2018. Antimicrobial activity of five essential oils against bacteria and fungi responsible for urinary tract infections. Molecules 23 (7), 1668.
Ebenyi, L.N., Ibiam, U.A., Aja, P.M., 2012. Effects of *Allium sativum* extract on paracetamol induced hepatotoxicity in albino rats. IRJBB 2, 93–97.
Edenharder, R., Grünhage, D., 2003. Free radical scavenging abilities of flavonoids as mechanism of protection against mutagenicity induced by tert-butyl hydroperoxide or cumene hydroperoxide in *Salmonella typhimurium* TA102. Mutat. Res. 540, 1–18.
Eftekhar, N., Moghimi, A., Mohammadian Roshan, N., Saadat, S., Boskabady, M.H., 2019. Immunomodulatory and anti-inflammatory effects of hydro-ethanolic extract of *Ocimum basilicum* leaves and its effect on lung pathological changes in an ovalbumin-induced rat model of asthma. BMC Compl. Alternative Med. 19 (1), 349.
El-Banna, H., Solimanand, M., Al-Wabel, N., 2013. Hepatoprotective effects of Thymus and Salvia essential oils on paracetamol induced toxicity in rats. J. Physiol. Pharmacol. Adv. 3, 41–47.
El-makawy, A., Ibrahim, F.M., Mabrouk, D.M., Abdel-Aziem, S.H., Sharaf, H.A., Ramadan, M.F., 2020. Efficiency of turnip bioactive lipids in treating osteoporosis through activation of Osterix and suppression of Cathepsin K and TNF-α signaling in rats. Environ. Sci. Pollut. Res. 27, 20950–20961.
Eratte, D., Wang, B., Dowling, K., Barrow, C.J., Adhikari, B.P., 2014. Complex coacervation with whey protein isolate and gum Arabic for the microencapsulation of omega-3 rich tuna oil. Food Funct. 5, 2743–2750.
Fahmy, H.M., Mohamed, F.M., Marzouq, M.H., Mustafa, A.B., Alsoudi, A.M., Ali, O.A., Mohamed, M.A., Mahmoud, F.A., 2018. Review of green methods of iron nanoparticles synthesis and applications. Bio. Nano Sci. 8, 491–503.
Fernández-Bertólez, N., Costa, C., Bessa, M.J., Park, M., Carriere, M., Dussert, F., Teixeira, J.P., Pásaro, E., Laffon, B., Valdiglesias, V., 2019. Assessment of oxidative damage induced by iron oxide nanoparticles on different nervous system cells. Mutat. Res. 845, 402989.
Fitsiou, E., Pappa, A., 2019. Anticancer activity of essential oils and other extracts from aromatic plants grown in Greece. Antioxidants 8, 290.
Florencia, I., María, C., María, S., van Raap, F., Benavides, M., Patricia, M., 2016. Impact of magnetite iron oxide nanoparticles on wheat (*Triticum aestivum* L.) development: evaluation of oxidative damage. Environ. Exp. Bot. 131.
Gad, A.S., Khadrawy, Y.A., El-Nekeety, A.A., Mohamed, S.R., Hassan, N.S., Abdel-Wahhab, M.A., 2011. Antioxidant activity and hepatoprotective effects of whey protein and *spirulina* in rats. Nutrition 27 (5), 582–589.
Gandhi, M., Aggarwal, M., Puri, S., Singla, S.K., 2013. Prophylactic effect of coconut water (Cocosnucifera L.) on ethylene glycol induced nephrocalcinosis in male Wistar rat. Int. Braz J. Urol. 39, 108–117.
Garcia-Fernandez, J., Turiel, D., Bettmer, J., Jakubowski, N., Panne, U., RivaGarcia, L., Llopis, J., Sanchez Gonzalez, C., Montes-Bayon, M., 2020. *In vitro* and *in situ* experiments to evaluate the biodistribution and cellular toxicity of ultrasmall iron oxide nanoparticles potentially used as oral iron supplements. Nanotoxicology 14, 1–16.
Ghasemi Pirbalouti, A., Malekpoor, F., Salimi, A., 2017. Chemical composition and yield of essential oil from two Iranian species of basil (*Ocimum ciliatum* and *Ocimum basilicum*). Trends Phytochem. Res. 1, 3–8.
Gibb, R.I., Taylor, D.D., Wan, T., O'Connor, D.M., Doeriog, D.L., GerHel-Taylor, T., 1997. Apoptosis as a measure of chemosensitivity to cisplatin and taxol therapy in ovarian cancer cell lines. Gynecol. Oncol. 65, 13–22.
Goula, A.M., Adamopoulos, K.G., 2012. A method for pomegranate seed application in food industries: seed oil encapsulation. Food Bioprod. Process. 90 (4), 639–652.
Hafiz, S.M., Kulkarni, S.S., Thakur, M.K., 2018. *In-vivo* toxicity assessment of biologically synthesized iron oxide nanoparticles in Zebrafish (*Danio rerio*). Biosci. Biotech. Res. Asia 15 (2), 419–425.
Hasanuzzaman, M., Borhannuddin Bhuyan, M.H.M., Zulfiqar, F., Raza, A., Mohsin, S.M., Al Mahmud, J., Fujita, M., Fotopoulos, V., 2020. Reactive oxygen species and antioxidant defense in plants under abiotic stress: revisiting the crucial role of a universal defense regulator. Antioxidants 9, 681.
Hassan, M.E., Hassan, R.R., Diab, K.A., El-Nekeety, A.A., Hassan, N.S., Abdel-Wahhab, M.A., 2021. Nanoencapsulation of thyme essential oil: a new avenue to enhance its protective role against oxidative stress and cytotoxicity of zinc oxide nanoparticles in rats. Environ. Sci. Pollut. Res. Int.
Helm, J.S., Rudel, R.A., 2020. Adverse outcome pathways for ionizing radiation and breast cancer involve direct and indirect DNA damage, oxidative stress, inflammation, genomic instability, and interaction with hormonal regulation of the breast. Arch. Toxicol. 94 (5), 1511–1549.
Huo, M., Cui, X., Xue, J., Chi, G., Gao, R., Deng, X., Guan, S., Wei, J., Soromou, L.W., Feng, H., Wang, D., 2013. Anti-inflammatory effects of linalool in RAW 264.7 macrophages and lipopolysaccharide-induced lung injury model. J. Surg. Res. 180, 47–54.
Jinapong, N., Suphantharika, M., Jammong, P., 2008. Production of instant soymilk powders by ultrafiltration, spray drying and fluidized bed agglomeration. J. Food Eng. 84, 194–205.
Jothirethinam, A., Prathiba, S., Shanthi, N., Arunkumar, K., 2015. Green synthesized silver nanoparticles prepared from the antimicrobial crude extracts of two brown seaweeds against plant pathogens. Am. J. Nanotechnol. 6 (2), 31.
Karabela, S.P., Kairi, C.A., Magkouta, S., Psallidas, I., Moschos, C., Stathopoulos, I., Zakynthinos, S.G., Roussos, C., Kalomenidis, I., Stathopoulos, G.T., 2011. Neutralization of tumor necrosis factor bioactivity ameliorates urethane-induced pulmonary oncogenesis in mice. Neoplasia 13 (12), 1143–1151.
Khan, I., Saeed, K., IKhan, I., 2019. Nanoparticles: properties, applications and toxicities Arab. J. Chem. 12 (7), 908–931.
Kim, E.H., Shim, B., Kang, S., Jeong, G., Lee, J.S., Yu, Y., Chun, M., 2009. Anti-inflammatory effects of *Scutellaria baical ensis* extract via suppression of immune modulators and MAP kinase signaling molecules. J. Ethnopharmacol. 126, 320–331.
Krzywoszyńska, K., Witkowska, D., Swiatek-Kozlowska, J., Szebesczyk, A., Kozłowski, H., 2020. General aspects of metal ions as signaling agents in health and disease. Biomolecules 10 (10), 1417.
Kulkarni, S., Mohanty, N., Kadam, N.N., Swain, N., Thakur, M., 2020. Green synthesis to develop iron-nano formulations and its toxicity assays. J. Pharmacopuncture 23 (3), 165–172.
Lammari, N., Louaer, O., Meniai, A.H., Elaissari, A., 2020. Encapsulation of essential oils via nanoprecipitation process: overview, progress, challenges and prospects. Pharmaceutics 12 (5), 431.
Li, J., Zhang, X., Huang, H., 2014. Protective effect of linalool against lipopoly-saccharide/d-galactosamine-induced liver injury in mice. Int. Immunopharm. 23, 523–529.
Liang, R., Xu, S., Shoemaker, C.F., Li, Y., Zhong, F., Huang, Q., 2012. Physical and antimicrobial properties of peppermint oil nanoemulsions. J. Agric. Food Chem. 60, 7548–7555.
Limaye, P.V., Raghuram, N., Sivakami, S., 2003. Oxidative stress and gene expression of antioxidant enzymes in the renal cortex of streptozotocin induced diabetic rats. Mol. Cell. Biochem. 243, 147–152.
Lin, C.C., Hsu, Y.F., Lin, T.C., Hsu, F.L., Hsu, H.Y., 1998. Antioxidant and hepato-protective activity of Punicalagin and Punicalin on carbon tetra chloride induced liver damage in rats. J. Pharm. Pharmacol. 50 (7), 789–794.
Litvinov, D., Mahini, H., Garelnabi, M., 2012. Antioxidant and anti-inflammatory role of paraoxonase 1: implication in arteriosclerosis diseases. N. Am. J. Med. Sci. 4, 523–532.
Livak, K.J., Schmittgen, T.D., 2001. Analysis of relative gene expression data using real-time quantitative PCR and the 2(-Delta Delta C (T)) method. Methods 25 (4), 402–408.
Lu, T., Xu, Y., Mericle, M.T., Mellgren, R.L., 2002. Participation of the conventional calpains in apoptosis. Biochim. Biophys. Acta 1590, 16–26.
Mahbubul, I.M., 2019. Stability and dispersion characterization of nanofluid.

Majdi, C., Pereira, C., Dias, M.I., Calhelha, R.C., Alves, M.J., Rhourri-Frih, B., Charrouf, Z., Barros, L., Amaral, J.S., Ferreira, I.C.F.R., 2020. Phytochemical characterization and bioactive properties of cinnamon basil (*Ocimum basilicum* cv. 'Cinnamon') and lemon basil (*Ocimum*×*citriodorum*). Antioxidants 9 (5), 369.

Malhotra, N., Lee, J.S., Liman, R.A.D., Ruallo, J.M.S., Villaflores, O.B., Ger, T.R., Hsiao, C.D., 2020. Potential toxicity of iron oxide magnetic nanoparticles: a review. Molecules 25 (14), 3159.

Malvindi, M.A., Matteis, V.D., Galeone, A., Brunetti, V., Anyfantis, G.C., Athanassiou, A., Cingolani, R., Pompa, P.P., 2014. Toxicity assessment of silica coated iron oxide nanoparticles and biocompatibility improvement by surface engineering. PloS One 9 (1), e85835.

McClements, D.J., Rao, J., 2011. Food-grade nanoemulsions: formulation, fabrication, properties, performance, biological fate, and potential toxicity. Crit. Rev. Food Sci. Nutr. 51 (4), 285–330.

Minj, S., Anand, S., 2020. Whey proteins and its derivatives: bioactivity, functionality, and current applications. Dairy 1 (3), 233–258.

Mohamed, M.I., Mohammad, K.A., Abdul Razak, H.R., Saad, W.M., 2015. Nanotoxic profiling of novel iron oxide nanoparticles functionalized with perchloric acid and SiPEG as a radiographic contrast medium. BioMed Res. Int. 1–7.

Mohammed, E.T., Hashem, K.S., Abdelazem, A.Z., Foda, F.A.M.A., 2020. Prospective protective effect of ellagic acid as a SIRT1 activator in iron oxide nanoparticle-induced renal damage in rats. Biol. Trace Elem. Res. 198, 177–188.

Mohammed, L., Gomaa, H.G., Ragab, D., Zhu, J., 2017. Magnetic nanoparticles for environmental and biomedical applications: a review. Particuol 30, 1–14.

Nasrin, K., Saeed, N., Mir, P., Zahra, E., Rezvan, N., Abolghasem, E., 2018. Hepatotoxicity and nephrotoxicity of quercetin, iron oxide nanoparticles, and quercetin conjugated with nanoparticles in rats. Comp. Clin. Pathol. 27.

Nemmar, A., Beegam, S., Yuvaraju, P., Yasin, J., Tariq, S., Attoub, S., Ali, B.H., 2016. Ultrasmall superparamagnetic iron oxide nanoparticles acutely promote thrombosis and cardiac oxidative stress and DNA damage in mice. Part. Fibre Toxicol. 13, 22.

Nikolić, B., Mitić-Ćulafić, D., Vuković-Gačić, B., Knežević-Vukčević, J., 2019. Plant monoterpenes camphor, eucalyptol, thujone, and DNA repair. In: patel, V., Preedy, V. (Eds.), Handbook of Nutrition, Diet, and Epigenetics. Springer, Cham.

Noello, C., Carvalho, A.G.S., Silva, V.M., Hubinger, M.D., 2016. Spray dried microparticles of chia oil using emulsion stabilized by whey protein concentrate and pectin by electrostatic deposition. Food Res. Int. 89 (1), 549–557.

Noori, A., Parivar, K., Modaresi, M., Messripour, M., Yousefi, M.H., Amiri, G.R., 2011. Effect of magnetic iron oxide nanoparticles on pregnancy and testicular development of mice. Afr. J. Biotechnol. 10, 1221–1227.

Olugbade, T.A., Kolipha-Kamara, M.I., Elusiyan, C.A., Onawunmi, G.O., Ogundaini, A.O., 2017. Essential oil chemotypes of three ocimum species found in Sierra Leone and Nigeria. Med. Aromatic Plants 6, 1–6.

Paramasivan, P., Kankia, I.H., Langdon, S.P., Deeni, Y.Y., 2019. Emerging role of nuclear factor erythroid 2-related factor 2 in the mechanism of action and resistance to anticancer therapies. Cancer Drug Resist. 2, 490–515.

Parivar, K., Fard, F.M., Bayat, M., Alavian, S.M., Motavaf, M., 2016. Evaluation of iron oxide nanoparticles toxicity on liver cells of BALB/c rats. Iran. Red Crescent Med. J. 18 (1), e28939.

Rafael, T.M., Yolanda, G.R., Patricia, R.C., Alfredo, S.M., Joel, L.M., Alejandra, O.Z., Rafael, S.G., 2018. Antioxidant activity of the essential oil and its major terpenes of *Satureja macrostema* (Moc. and Sessé ex Benth). Briq. Pharmacogn. Mag. 13, S875–S880.

Rashidian, A., Roohi, P., Mehrzadi, S., Ghannadi, A.R., Minaiyan, M., 2016. Protective effect of *Ocimum basilicum* essential oil against acetic acid induced colitis in rats. J. Evid. Based. Complement. Altern. Med. 21 (4), NP36–NP42.

Reddy, U.A., Prabhakar, P.V., Mahboob, M., 2017. Biomarkers of oxidative stress for *in vivo* assessment of toxicological effects of iron oxide nanoparticles. Saudi J. Biol. Sci. 24, 1172–1180.

Rezzoug, M., Bakchiche, B., Gherib, A., Roberta, A., Guido, F., Kilinçarslan, Ö., Mammadov, R., Bardaweel, S.K., 2019. Chemical composition and bioactivity of essential oils and ethanolic extracts of *Ocimum basilicum* L. and *Thymus algeriensis* Boiss and Reut from the Algerian Saharan Atlas. BMC Compl. Alternative Med. 19 (1), 146.

Rim, K.T., Song, S.W., Kim, H.Y., 2013. Oxidative DNA damage from nanoparticle exposure and its application to workers' health: a Literature Review. Saf. Health Work. 4 (4), 177–186.

Roger, B., Lagarce, F., Garcion, E., Benoit, J.P., 2010. Biopharmaceutical parameters to consider in order altering the fate of nanocarriers after oral delivery. Nanomedicine 5 (2), 287–306.

Sadat, M., Jahan, S.T., Haddadi, A., 2016. Effects of size and surface charge of polymeric nanoparticles on *in vitro* and *in vivo* applications. J. Biomaterials Nanobiotechnol. 7, 91–108.

Sadauskas, E., Wallin, H., Stoltenberg, M., Vogel, U., Doering, P., Larsen, A., Danscher, G., 2007. Kupffer cells are central in the removal of nanoparticles from the organism. Part. Fibre Toxicol. 4, 10.

Sandra, F., Saidi, S., Richard, H., Ellen, A., 2019. Essential oils and their applications-A mini review. Adv. Nutr. Food Sci. 4, 1–13.

Shen, Y., Huang, Z., Liu, X., Qian, J., Xu, J., Yang, X., Sun, A., Ge, J., 2015. Iron-induced myocardial injury: an alarming side effect of superparamagnetic iron oxide nanoparticles. J. Cell Mol. Med. 19, 2032–2035.

Singh, N., Jenkins, G.J.S., Asadi, R., Doak, S.H., 2010. Potential toxicity of superparamagnetic iron oxide nanoparticles (SPION). Nano Rev. 1, 5358.

Soenen, S., De Cuyper, J., Smedt, M., Braeckmans, S.C., 2012. Investigating the toxic effects of iron oxide nanoparticles. Methods Enzymol. 509.

Sripetchwandee, J., Wongjaikam, S., Krintratun, W., Chattipakorn, N., Chattipakorn, S.C., 2016. A combination of an iron chelator with an antioxidant effectively diminishes the dendritic loss, tau-hyperphosphorylation, amyloids-βaccumulation and brain mitochondrial dynamic disruption in rats with chronic iron-overload. Neuroscience 332, 191–202.

Talesh, S., Kazem Koohi, M., Zayerzadeh, E., Hasan, J., Shabanian, M., 2019. Acute toxicity investigation regarding clinical and pathological aspects following repeated oral administration of iron oxide nanoparticles in rats. Nanomed. Res. J. 4 (4), 228–233.

Tamoghna, G., Santosh, S., Amit, G., Alok, K., Piyush, K., Ajit, Y., Ranjana, P., Naveen, N., 2018. A combination of linalool, vitamin C, and copper synergistically trigger reactive oxygen species, DNA damage and inhibits *Salmonella enterica* subsp. enterica serovar Typhi and *Vibrio fluvialis*. Appl. Environ. Microbiol. 85.

Theodosiou, E., Purchartová, K., Stamatis, H., Kolisis, F., Křen, V., 2014. Bioavailability of silymarin flavonolignans: drug formulations and biotransformation. Phytochemistry Rev. 13, 1–18.

Toyokuni, S., 2009. Role of iron in carcinogenesis: cancer as a ferrotoxic disease. Canc. Sci. 100 (1), 9–16.

Wang, J., Chen, Y., Chen, B., Ding, J., Xia, G., Gao, C., Cheng, J., Jin, N., Zhou, Y., Li, X., Tang, M., Wang, X.M., 2010. Pharmacokinetic parameters and tissue distribution of magnetic Fe_3O_4 nanoparticles in mice. Int. J. Nanomed. 5, 861.

Wonsawat, W., Panprom, Y., 2016. Green synthesis and characterization of iron nanoparticles from holy basil leaves and mint leaves key. Eng. Mater. 675–676, 121–124.

Yacout, G.A., Elguindy, N.M., El Azab, E.F., 2012. Hepatoprotective effect of basil (*Ocimum basilicum* L.) on CCl_4-induced liver fibrosis in rats. Afr. J. Biotechnol. 11 (90), 15702–15711.

Yarjanli, Z., Ghaedi, K., Esmaeili, A., Rahgozar, S., Zarrabi, A., 2017. Iron oxide nanoparticles may damage to the neural tissue through iron accumulation, oxidative stress, and protein aggregation. BMC Neurosci. 18 (1), 51.

Yousef, M.I., Mutar, T.F., Kamel, M.A.E., 2019. Hepato-renal toxicity of oral sub-chronic exposure to aluminum oxide and/or zinc oxide nanoparticles in rats. Toxicol. Rep. 6, 336–346.

Zhu, L., Zhou, Z., Mao, H., Yang, L., 2017. Magnetic nanoparticles for precision oncology: the ranostic magnetic iron oxide nanoparticles for image-guided and targeted cancer therapy. Nanomedicine 12 (1), 73–87.

Zhu, X., Tian, S., Cai, Z., 2012. Toxicity assessment of iron oxide nanoparticles in zebrafish (*Danio rerio*) early life stages. PloS One 7 (9), e46286.